SEISMIC WAVES ESTIMATION AND WAVE FIELD DECOMPOSITION WITH FACTOR GRAPHS

Stefano Maranò[⋆] *Christoph Reller*[†] *Donat Fäh*[⋆] *Hans-Andrea Loeliger*[†]

[⋆] ETH Zurich, Swiss Seismological Service, 8092 Zürich
[†] ETH Zurich, Dept. Information Technology & Electr. Eng., 8092 Zürich

ABSTRACT

Physical wave fields are often described by means of a vector field. Advances in sensor technology enable us to collect an increasing number of measurement at the same location (e.g. direction, polarization, translation, and rotation). One question arising naturally is how to properly process such large and diverse information, possibly from sensors of different kinds. In this paper we propose a technique for the analysis of vector wave fields and show an application to the seismic wave field. The contributions of this paper are the following: i) We provide a framework to perform maximum likelihood parameter estimation of any wave type, modeling jointly all the measurements and parameters; ii) In the same framework, we address wave superposition by gradually decomposing the wave field; iii) We also propose an iterative algorithm for noise variance estimation.

Index Terms— Array signal processing, factor graph, seismic waves.

1. INTRODUCTION AND SYSTEM MODEL

In this paper, we propose a technique for the analysis of vector wave fields. Our primary goal is the estimation of wave field parameters based on discrete-time observations from a sensor array. In particular, we are concerned with sensors measuring vector quantities such as direction, polarization, translation, and rotation. In practical applications several waves may be simultaneously present. Our further goal is to decompose the wave field by separating the contributions of different waves.

In the analysis of physical wave fields we are typically interested in studying vector fields of the form $\mathbf{u}(\boldsymbol{p},t):\mathbb{R}^4\rightarrow\mathbb{R}^C$. The quantity $\mathbf{u}\in\mathbb{R}^C$ depends on the position $\boldsymbol{p}\in\mathbb{R}^3$, time t, and wave field parameters $\boldsymbol{\theta}$. The value of C depends on the sensor we use to measure the wave field. The wave field is measured by means of an array of N sensors. We call $L=NC$ the overall number of channels. In presence of multiple sources, M waves coexist at the same time in the wave field. Assuming a linear medium, the superposition of these waves is measured in each channel. We now restrict our analysis to a monochromatic wave field with known angular frequency ω. In this setting, we model the signal on each channel as the sum of scaled and delayed copies of underlying reference sinusoids

$$u^{(\ell)}(\boldsymbol{p},t)=\sum_{m=1}^{M}\rho_\ell^{(m)}\rho_0^{(m)}\cos\left(\omega t+\phi_\ell^{(m)}+\phi_0^{(m)}\right)\,. \quad (1)$$

With this signal model, the m-th wave is parametrized by the amplitudes and phases $\boldsymbol{\eta}_m\triangleq\{\rho_\ell^{(m)},\phi_\ell^{(m)}\}_{\ell=0,\dots,L}$. The m-th reference sinusoid $\rho_0^{(m)}\cos(\omega t+\phi_0^{(m)})$ is defined by $\rho_0^{(m)}$ and $\phi_0^{(m)}$. However, our interest lies in the estimation of wave field parameters $\boldsymbol{\theta}_m$ governing the amplitudes and the phases measured at the different sensors. The parameters $\boldsymbol{\eta}$ and $\boldsymbol{\theta}$ are related by means of a mapping $\Gamma:\boldsymbol{\theta}\rightarrow\boldsymbol{\eta}$. In general, $\{\rho_\ell,\phi_\ell\}_{\ell=1,\dots,L}$ can be influenced by different quantities such as velocity and direction of propagation (i.e., by the wave vector), wave polarization, wave attenuation, sensor directional gain, instrument response, and others.

Each signal is measured as

$$Y_k^{(\ell)}=u^{(\ell)}(\boldsymbol{p},t_k)+Z_k^{(\ell)} \quad (2)$$

at times t_k and is corrupted by Gaussian noise $Z_k^{(\ell)}\overset{\text{iid}}{\sim}\mathcal{N}\left(0,\sigma_\ell^2\right)$.

2. SEISMIC WAVE FIELD

The seismic wave field (i.e., elastic waves propagating through the earth) offers an interesting example since it presents the simultaneous presence of functionally different and completely decoupled wave types [1].

To measure seismic waves, we deploy an array of triaxial ($C=3$) seismometers on the surface of the earth[1]. Each sensor measures the ground velocity along the direction of the axes of the coordinate system x, y, and z. For the sake of simplicity, we provide wave equations of the displacement field $\mathbf{u}$, despite the actual measurement is the velocity field $\frac{\partial\boldsymbol{u}}{\partial t}$. The displacement can be described by the vector field

$$\boldsymbol{u}(\boldsymbol{p},t)\triangleq(u_x(\boldsymbol{p},t),u_y(\boldsymbol{p},t),u_z(\boldsymbol{p},t)):\mathbb{R}^4\rightarrow\mathbb{R}^3\,.$$

[1]We restrict our interest to small aperture arrays and work with a flat earth model. We use a three-dimensional, right-handed Cartesian coordinate system with the z axis pointing upward. The azimuth ψ is measured counterclockwise from the x axis.

In this paper, we study waves propagating near the surface of the earth and having a direction of propagation lying on the horizontal plane $z = 0$. The wave field is composed of the superposition of several Rayleigh and Love waves. The wave equations we describe hereafter are valid for $z = 0$ and for plane wave fronts. Rayleigh waves exhibit an elliptical particle motion confined in the vertical plane perpendicular to the earth's surface and defined by the direction of propagation of the wave. The particle displacement generated by a single Rayleigh wave at position and time $(\boldsymbol{p}, t)$ is

$$\begin{aligned} u_x(\boldsymbol{p},t) &= \alpha \sin\xi \cos\psi \cos(\omega t - \boldsymbol{\kappa}^{\mathrm{T}}\boldsymbol{p} + \varphi) \\ u_y(\boldsymbol{p},t) &= \alpha \sin\xi \sin\psi \cos(\omega t - \boldsymbol{\kappa}^{\mathrm{T}}\boldsymbol{p} + \varphi) \\ u_z(\boldsymbol{p},t) &= \alpha \cos\xi \cos(\omega t - \boldsymbol{\kappa}^{\mathrm{T}}\boldsymbol{p} + \frac{\pi}{2} + \varphi)\,. \end{aligned} \tag{3}$$

The direction of propagation of a wave is given by the wave vector $\boldsymbol{\kappa} \triangleq \kappa\,(\cos\psi, \sin\psi, 0)^{\mathrm{T}}$, whose magnitude κ is the wavenumber. The quantity $\tan\xi$ is called ellipticity of the Rayleigh wave and determines the eccentricity and the sense of rotation of the particle motion.

Love waves exhibit a particle motion confined on the horizontal plane, the particle oscillates transversely with respect to the direction of propagation. The particle displacement generated by a single Love wave is

$$\begin{aligned} u_x(\boldsymbol{p},t) &= -\alpha \sin\psi \cos(\omega t - \boldsymbol{\kappa}^{\mathrm{T}}\boldsymbol{p} + \varphi) \\ u_y(\boldsymbol{p},t) &= \alpha \cos\psi \cos(\omega t - \boldsymbol{\kappa}^{\mathrm{T}}\boldsymbol{p} + \varphi) \\ u_z(\boldsymbol{p},t) &= 0\,. \end{aligned} \tag{4}$$

With these wave equations in mind, we can now give an explicit expression for the mapping[2]. Let $\boldsymbol{p}_n$ be the known position of the n-th sensor. The mapping $\Gamma^{(\mathrm{R})} : \boldsymbol{\theta}^{(\mathrm{R})} \to \boldsymbol{\eta}$, with $\boldsymbol{\theta}^{(\mathrm{R})} \triangleq (\alpha, \varphi, \kappa, \psi, \xi)$, specialized to the Rayleigh wave, is

$$\begin{aligned} (\rho_0, \phi_0) &= (\alpha, \varphi) \\ \big(\rho_{(n,1)}, \phi_{(n,1)}\big) &= \big(\sin\xi\cos\psi, -\boldsymbol{\kappa}^{\mathrm{T}}\boldsymbol{p}_n\big) \\ \big(\rho_{(n,2)}, \phi_{(n,2)}\big) &= \big(\sin\xi\sin\psi, -\boldsymbol{\kappa}^{\mathrm{T}}\boldsymbol{p}_n\big) \\ \big(\rho_{(n,3)}, \phi_{(n,3)}\big) &= \Big(\cos\xi, -\boldsymbol{\kappa}^{\mathrm{T}}\boldsymbol{p}_n + \frac{\pi}{2}\Big) \end{aligned}$$

for $n = 1, \ldots, N$. Analogously, for a Love wave we define the mapping $\Gamma^{(\mathrm{L})} : \boldsymbol{\theta}^{(\mathrm{L})} \to \boldsymbol{\eta}$, with $\boldsymbol{\theta}^{(\mathrm{L})} \triangleq (\alpha, \varphi, \kappa, \psi)$ as

$$\begin{aligned} (\rho_0, \phi_0) &= (\alpha, \varphi) \\ \big(\rho_{(n,1)}, \phi_{(n,1)}\big) &= \big(-\sin\psi, -\boldsymbol{\kappa}^{\mathrm{T}}\boldsymbol{p}_n\big) \\ \big(\rho_{(n,2)}, \phi_{(n,2)}\big) &= \big(\cos\psi, -\boldsymbol{\kappa}^{\mathrm{T}}\boldsymbol{p}_n\big) \\ \big(\rho_{(n,3)}, \phi_{(n,3)}\big) &= (0, 0)\ . \end{aligned}$$

[2]We use (n, c) to refer to the c-th component of the n-th sensor instead of (ℓ) for the ℓ-th channel. The mapping between (n, c) and (ℓ) is bijective.

3. PROPOSED TECHNIQUE

3.1. Factor Graph

The probability density function of the observations y is

$$p(y|\boldsymbol{\eta}) = \prod_{\ell=1}^{L}\prod_{k=1}^{K} \frac{1}{\sqrt{2\pi\sigma_\ell^2}} \mathrm{e}^{-\left(y_k^{(\ell)} - u_k^{(\ell)}\right)^2 / 2\sigma_\ell^2}\,, \tag{5}$$

where we rely on K discrete-time observations for each channel and define $y \triangleq \{y_k^{(\ell)}\}_{\ell=1,\ldots L}^{k=1,\ldots,K}$ and $u_k^{(\ell)} \triangleq u^{(\ell)}(\boldsymbol{p}_\ell, t_k)$.

Instead of computing (5), we model it by means of a factor graph [2]. For every signal $Y_k^{(\ell)}$, we consider a second-order state space model with state $\boldsymbol{X}_k^{(\ell)} \in \mathbb{R}^2$

$$\begin{aligned} \boldsymbol{X}_{k-1}^{(\ell)} &= \mathbf{A}_k \boldsymbol{X}_k^{(\ell)} \\ Y_k^{(\ell)} &= \boldsymbol{C}\boldsymbol{X}_k^{(\ell)} + Z_k^{(\ell)}\,, \end{aligned}$$

where $\mathbf{A}_k \triangleq \mathrm{rotm}(\omega(t_{k-1} - t_k))$ is a clockwise rotation matrix $\mathrm{rotm}(\beta) \triangleq \left(\begin{smallmatrix} \cos\beta & -\sin\beta \\ \sin\beta & \cos\beta \end{smallmatrix}\right)$, and the measurement matrix $\boldsymbol{C} \triangleq (0, -\omega)$ accounts for the derivative $\frac{\partial \boldsymbol{u}}{\partial t}$. The corresponding factor graph is depicted in Fig. 1(a).

Using a glue factor, we constrain the final states of every channel with the following L equations

$$\boldsymbol{X}_K^{(\ell)} = \sum_{m=1}^{M} \mathbf{H}_\ell^{(m)} \boldsymbol{u}_m = \sum_{m=1}^{M} \boldsymbol{S}_\ell^{(m)}\,, \tag{6}$$

where $\mathbf{H}_\ell^{(m)} \triangleq \rho_\ell^{(m)}\,\mathrm{rotm}(\phi_\ell^{(m)})$ are the constraint matrices, $\boldsymbol{S}_\ell^{(m)} \triangleq \mathbf{H}_\ell^{(m)}\boldsymbol{u}_m$ is the contribution on the ℓ-th channel of the m-th wave, and the state vector of the m-th reference sinusoid is $\boldsymbol{u}_m \triangleq \rho_0^{(m)}(\cos(\omega t_K + \phi_0^{(m)}), \sin(\omega t_K + \phi_0^{(m)}))^{\mathrm{T}}$. The corresponding factor graph is shown in Fig. 1(b), where $\boldsymbol{S}_\ell^{\not m}$ represents the contribution on the ℓ-th channel of all but the m-th wave. The overall graph is shown in Fig. 1(c).

Using the sum-product algorithm on the factor graph we can compute the likelihood function $p(y|\boldsymbol{\eta})$. We use Gaussian messages parametrized by mean vector, covariance matrix, and scale factor. We provide a detailed description in [3].

3.2. Parameter Estimation

We now focus on the estimation of wave field parameters $\boldsymbol{\theta}$, in the case of a single wave ($M = 1$) and known noise variance.

We introduce the set $\mathcal{G}$ of all the parameter mappings of interest. The maximum likelihood (ML) estimate of wave field parameter is given by

$$(\hat{\Gamma}, \hat{\boldsymbol{\theta}}) \in \underset{\Gamma\in\mathcal{G}, \boldsymbol{\theta}\in\mathrm{dom}\,\Gamma}{\mathrm{argmax}}\ p\big(y\big|\Gamma(\boldsymbol{\theta})\big)\,. \tag{7}$$

This maximization allows us to find the most likely wave type with the most likely parameters.

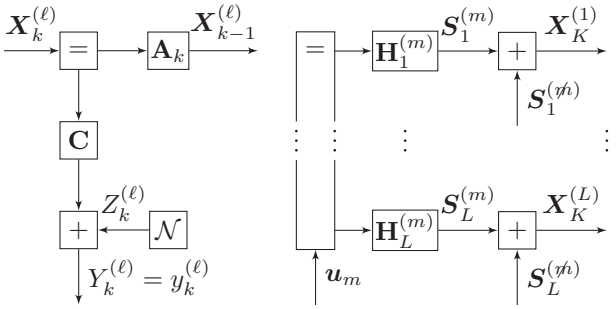

(a) State space model. (b) Glue factor g.

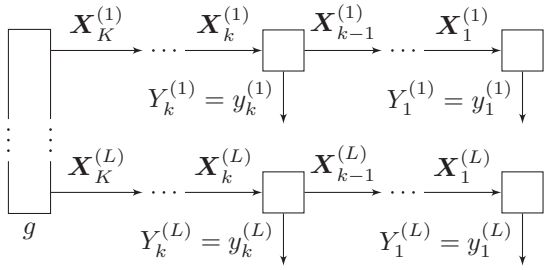

(c) Overall factor graph.

Fig. 1. Building blocks and overall view of the factor graph of (5).

3.3. Wave Field Decomposition

When $M > 1$, Eq. 6 captures the presence of multiple waves. However, because of the larger number wave field parameters, a joint maximization of the likelihood function might be impractical.

We propose to gradually increase the number of waves modeled by the graph and perform smaller maximizations on the wave field parameters of each wave separately. In practice, once we insert an estimate $\hat{\boldsymbol{s}}_\ell^{\not m}$ of $\boldsymbol{S}_\ell^{\not m}$, we perform the maximization over $\boldsymbol{\theta}_m$ as in (7). Each maximization increases the likelihood and convergence is guaranteed.

3.4. Noise Variance Estimation

The ML noise variance estimate is given by

$$\hat{\sigma}_\ell^2 = \frac{1}{K}\sum_{k=1}^{K}\left(y_k^{(\ell)} - \boldsymbol{C}\,\mathrm{rotm}\left(\omega(t_k - t_K)\right)\overrightarrow{\boldsymbol{m}}_{\boldsymbol{X}_K^{(\ell)}}\right)^2,$$

with $\overrightarrow{\boldsymbol{m}}_{\boldsymbol{X}_K^{(\ell)}} = \sum_{m=1}^{M}\mathbf{H}_\ell^{(m)}\overrightarrow{\boldsymbol{m}}_{\boldsymbol{U}_m}$. Since the messages $\overrightarrow{\boldsymbol{m}}_{\boldsymbol{U}_m}$ depend on $\hat{\sigma}_\ell^2$, this leads to an iterative algorithm where noise variance and messages are estimated iteratively.

4. NUMERICAL EXAMPLES

In the first example, we generate a synthetic wave field composed of two Rayleigh and two Love waves. The number of waves $M = 4$ is known. Waves are monochromatic at known frequency of 1 Hz. We use an array of 14 triaxial sensors, 500 samples, and 5 seconds of observation. Measurements are corrupted by additive white Gaussian noise, with different variance in each channel. We look for both Rayleigh and Love waves, i.e., $\mathcal{G} \triangleq \{\Gamma^{(\mathrm{R})}, \Gamma^{(\mathrm{L})}\}$. True wave field parameters are $\boldsymbol{\theta}_1^{(\mathrm{R})} = (0.9, 0, 0.03, \frac{\pi}{4}, \frac{\pi}{4})^{\mathrm{T}}$, $\boldsymbol{\theta}_2^{(\mathrm{R})} = (0.8, \frac{\pi}{4}, 0.03, \frac{\pi}{2}, \frac{\pi}{4})^{\mathrm{T}}$, $\boldsymbol{\theta}_3^{(\mathrm{L})} = (0.7, \frac{\pi}{3}, 0.04, -\frac{\pi}{4})^{\mathrm{T}}$, and $\boldsymbol{\theta}_4^{(\mathrm{L})} = (0.2, \pi, 0.04, \pi)^{\mathrm{T}}$. Noise variance and wave field parameters are unknown to the algorithm.

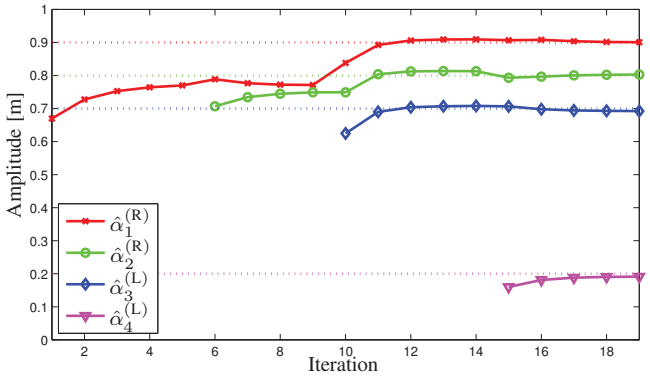

Fig. 2. Estimated amplitude at different iterations. The graph accounts for an additional wave at iteration 1, 6, 10, and 15.

Fig. 2 shows how the estimates of the amplitudes α converge toward their true values (dotted lines) after a sufficient number of iterations. The factor graph is enlarged to account for additional waves at iterations 6, 10, and 15 as the likelihood (not shown) converges to a stable value. Similarly, Fig. 3 shows the the estimates of noise variance σ_ℓ^2. Sudden decrease in estimated variance in the graph correspond to the inclusion of an additional wave in the graph.

Fig. 4 depicts $\log p\big(y\big|\Gamma^{(\mathrm{L})}(\boldsymbol{\theta}^{(\mathrm{L})})\big)$, as a function of wavenumber κ and azimuth ψ in polar coordinates (κ, ψ). In Fig. 4(a) it is possible to see at $\psi_3 = -\frac{\pi}{4}$ one stronger peak associated with the wave parametrized by $\boldsymbol{\theta}_3^{(\mathrm{L})}$ and no other strong peaks are visible. At iteration 14, only one Love wave remains in the wave field (the wave parametrized by $\boldsymbol{\theta}_4^{(\mathrm{L})}$) and the associated peak, located at $\psi_4 = \pi$, is now clearly visible, as shown in Fig. 4(b). At the last iteration, no more waves remain in the the residual wave field, Fig. 4(c).

We now use a more sophisticated synthetic wave field developed in the SESAME project [4, 5]. This synthetic dataset captures the complexity of the seismic wave field, accounting for the simultaneous presence of several seismic sources, emitting both short burst of energy and longer harmonic excitations. It is a wave field of *ambient vibrations*, where the wave field is dominated by surface waves (i.e., Rayleigh and Love waves) but also other waves are present (e.g., body waves and standing waves). We use an earth model

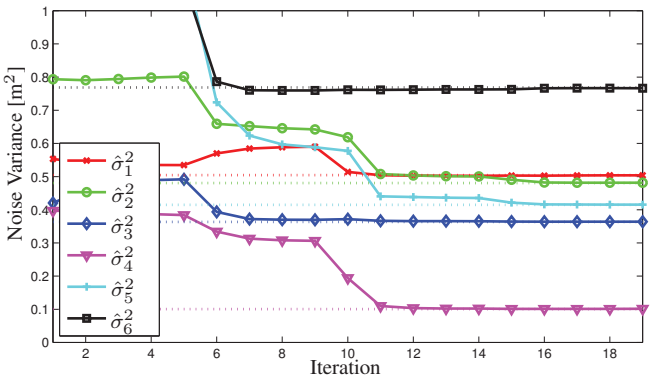

Fig. 3. Estimated noise variance at different iterations. Only six channels are shown.

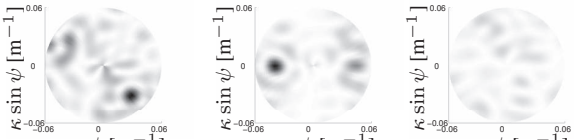

(a) Iteration 1 (b) Iteration 14 (c) Iteration 18

Fig. 4. Log-likelihood function of a Love wave.

of a layer with low seismic velocities over a half-space with higher velocities. We use 38 sensors and solely 10 seconds of recording. Different frequencies are processed independently. Of practical interest is the phase velocity dispersion of surface waves [1].

We define $\mathcal{G} \triangleq \{\Gamma^{(\mathrm{R})}\}$ and initially model a single Rayleigh wave, i.e., $M = 1$. In Fig. 5, the estimates of the wavenumbers κ (black dots) suggest the Rayleigh wave dispersion curves. For comparison, the theoretical dispersion curves are depicted by lines. In Fig. 6, the number of waves modeled is increased to $M = 3$. It is shown that increasing the number of waves modeled by the factor graph, allows to better retrieve the fundamental and the higher modes.

5. CONCLUSIONS

We have developed a technique to perform ML estimation of wave field parameter of any wave type. The technique accounts for different noise variance on each channel, by properly merging the information from sensors with different noise level. In the same framework, we address the superposition of multiple waves and show that wave field decomposition enables to detect weaker waves. We also propose an iterative algorithm for noise variance estimation. The technique accounts for arbitrary sensor positions and arbitrary sampling instants.

We show numerical examples on monochromatic signals and on a well-established dataset of the seismic wave field.

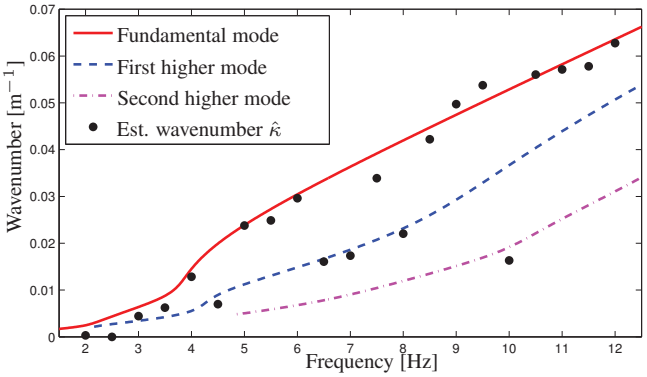

Fig. 5. Rayleigh wave dispersion curve, $M = 1$.

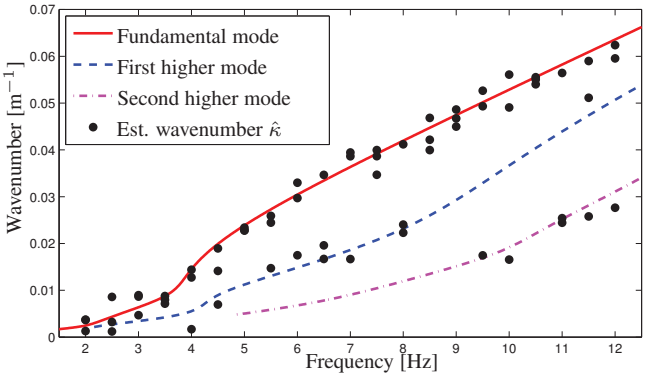

Fig. 6. Rayleigh wave dispersion curve, $M = 3$.

6. REFERENCES

[1] K. Aki and P. G. Richards, *Quantitative seismology*, A. Cox, Ed. W. H. Freeman and Company, 1980.

[2] H.-A. Loeliger, J. Dauwels, J. Hu, S. Korl, L. Ping, and F. R. Kschischang, "The factor graph approach to model-based signal processing," *Proc. IEEE*, vol. 95, no. 6, pp. 1295–1322, June 2007.

[3] C. Reller, H.-A. Loeliger, and S. Maranò, "Multi-sensor estimation and detection of phase-locked sinusoids," in *Proc. IEEE Int. Conf. Acoustics, Speech, and Signal Processing*, Prague, Czech Republic, May 2011.

[4] SESAME: Site effects assessment using ambient excitations. [Online]. Available: http://sesame-fp5.obs.ujf-grenoble.fr

[5] S. Bonnefoy-Claudet, C. Cornou, P.-Y. Bard, F. Cotton, P. Moczo, J. Kristek, and D. Fäh, "H/V ratio: a tool for site effects evaluation. results from 1-D noise simulations," *Geophys. J. Int.*, vol. 167, no. 2, pp. 827–837, Nov. 2006.